MAGNETNI GRADIOMETER Z ULTRAHLADNIMI ATOMI CEZIJA NA OSNOVI ENE SAME STERN-GERLACHOVE SLIKE

KATJA GOSAR

Fakulteta za matematiko in fiziko
Univerza v Ljubljani

Magnetno polje lahko merimo preko Larmorjeve precesije atomske magnetizacije. V članku je pojasnjena dinamika magnetizacije v magnetnih poljih, vključujoč Larmorjevo precesijo in Rabijeve oscilacije ter uporaba Stern-Gerlachove metode za zaznavanje projekcije magnetizacije hladnih cezijevih atomov. Predstavljena so eksperimentalna opažanja teh pojavov in demonstracija metode za merjenje ene komponente tenzorja magnetnega gradienta na osnovi ene same Stern-Gerlachove slike.

SINGLE-SHOT STERN-GERLACH MAGNETIC GRADIOMETER WITH ULTRACOLD CESIUM ATOMS

The magnetic field can be measured through Larmor precession of the atomic magnetization. In this article the dynamics of magnetization in magnetic fields is explained, including Larmor precession and Rabi oscillations, and the use of the Stern-Gerlach method to probe the magnetization projection of cold cesium atoms. Experimental observations of these phenomena are presented, including a demonstration of a magnetic gradiometer capable of measuring one component of the magnetic field gradient tensor in a single shot.

1. Introduction

Atomic vapour magnetometers are the most sensitive devices for measuring magnetic fields reaching sensitivities up to $10^{-15}\,\mathrm{T}/\sqrt{\mathrm{Hz}}$ [1]. The basic principle behind this type of magnetometers is the precession of spins in a magnetic field. The phenomenon is called Larmor precession and its frequency is proportional to the magnitude of the magnetic field. The idea for an optical magnetometer with atomic gas was proposed by Dehmelt in 1957 and experimentally demonstrated by Bell and Bloom in the same year [1]. In a typical atomic magnetometer the probe atoms are in a glass bulb at room temperature and the precession is observed through the rotation of the polarization of light due to the Faraday effect.

Techniques for cooling and trapping atoms, developed in the last decades of the last century, enable us to prepare clouds of atoms with temperatures close to absolute zero. Cold atoms are very suitable for use in precise measuring because of their long lifetimes and small Doppler broadening [2]. In magnetometry the limiting factor is usually the small sizes of atom clouds. The number of atoms in a cloud is typically an order of magnitude smaller than in cells with hot atom vapour, despite their large density. Consequently, signals proportional to the number of atoms are very small and difficult to measure. The sensitivity of cold magnetometers does not reach that of the best devices with hot atom vapours, but they are very suitable for measurements with a high spatial resolution, because of the small size of the clouds [1].

Typically, cold atom magnetometers use the same technique as room-temperature atomic vapour magnetometers to detect the signal – Faraday rotation. However, in case of cold atoms this is not the only option for detecting spin precession. The projection of the magnetization can be measured through the populations of Zeeman sublevels using the Stern-Gerlach method, as done in Ref. 3 to measure the magnetic field through Larmor precession. Another option is state-selective absorption imaging used in Ref. 4, where only the atoms that have left the initial magnetic sublevel are detected.

Sensors of the magnetic field and its gradient are used for a wide variety of applications from detecting anomalies in geomagnetic fields to measuring NMR signals and magnetic signals of the

brain and heart in medicine [1, 5]. The advantage of measuring the gradient is that it provides information about the magnetic field without the background magnetic noise. A basic gradiometer consists of two magnetometer probes separated in space and the magnetic gradient is derived by differentiating their output. This way any common-mode noise on the two probes cancels out.

Magnetic gradiometry using two clouds of cold atoms is demonstrated in Ref. 6. In their experiment the positions of the two clouds is variable, thus enabling the measurement of the whole gradient tensor. If an elongated atomic cloud is used instead of two separate clouds, this allows measurements of the spatial profile of the magnetic field. If the magnetic field was completely homogeneous, the whole cloud would precess in phase. But in a magnetic field gradient the precession frequency changes along the cloud, causing a helical or "corkscrew" spatial dependence of the magnetization direction observed in Refs. 7 and 8. A technique of measuring the magnetic gradient based on this observation is described in Ref. 4.

In the first part of this article, the theoretical principles behind magnetometry with cold cesium atoms using the Stern-Gerlach method are described. In the second part we present experiments done in the Cold atom laboratory at Jožef Stefan Institute, including a single-shot method of measuring one component of the magnetic field gradient tensor.

2. Theoretical description

2.1 Cesium atoms

Cesium is an alkali metal, hence it has only one valence electron. Its only stable isotope is ^{133}Cs.

The angular momentum of an atom is a sum of electron spin $\mathbf{S}$, electron orbital angular momentum $\mathbf{L}$ and the nuclear angular momentum $\mathbf{I}$. The energy levels of an atom are determined to first approximation by the electron orbital angular momentum quantum number L. These levels are split into the fine structure, which is a result of spin-orbit coupling and is described with the total electron angular momentum $\mathbf{J} = \mathbf{L} + \mathbf{S}$. A further splitting resulting in the hyperfine structure is a consequence of the coupling of $\mathbf{J}$ with the nuclear angular momentum $\mathbf{I}$, yielding the total atomic angular momentum $\mathbf{F} = \mathbf{J} + \mathbf{I}$.
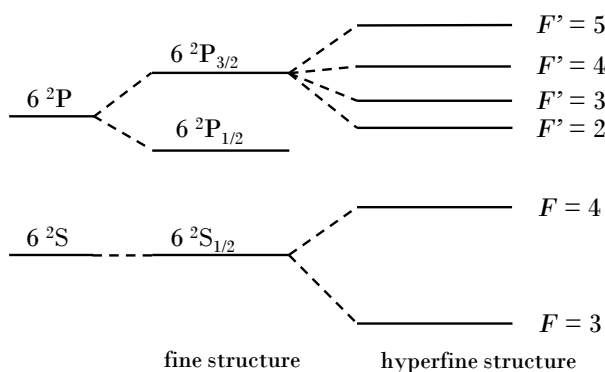

Figure 1. Energy levels of the ground and first excited state of cesium atoms. The energy splittings are not to scale. Adapted from [9].

In the cesium ground state the valence electron is in the orbital with $L = 0$ and has a spin $S = 1/2$, so the total electron angular momentum is $J = 1/2$. Because the nuclear angular momentum of cesium is $I = 7/2$, the hyperfine structure splits the ground state into levels $F = 4$ and $F = 3$, from which the latter has the lower energy. The energy level structure of the ground state and the first excited state of a cesium atom is shown in Figure 1.

2.2 Interaction of atoms with a magnetic field

Interaction of a magnetic dipole moment $\boldsymbol{\mu}$ with a magnetic field $\mathbf{B}$ is described by the addition of the Zeeeman term

$$H_B = -\boldsymbol{\mu} \cdot \mathbf{B} \tag{1}$$

to the Hamiltonian. The magnetic dipole moment of an atom is proportional to its total angular momentum $\mathbf{F}$ as $\boldsymbol{\mu} = \gamma \mathbf{F}$, where γ is the gyromagnetic ratio.

Each hyperfine level consists of $2F + 1$ magnetic sublevels, that are degenerate in the absence of an external magnetic field. In the presence of a magnetic field, the difference in energy of neighbouring sublevels is ΔE. The sublevels are described by the operator of projection of the total angular momentum on the quantization axis, that is the direction of the magnetic field. For the magnetic field in the z-direction, $\mathbf{B} = (0, 0, B_z)$, this operator is F_z and its eigenvalues are $\hbar m_F$, where m_F is a quantum number with $2F + 1$ possible values, ranging from $-F$ to F in steps of 1.

F is a good quantum number if the energy difference between Zeeman sublevels is small in comparison to the hyperfine splitting. In that case the Zeeman Hamiltonian can be written as

$$H_B = -\frac{\mu_B g_F}{\hbar} \mathbf{F} \cdot \mathbf{B}, \tag{2}$$

where g_F is the Landé g-factor. Comparing the equations (1) and (2), we can see that the gyromagnetic ratio is $\gamma = \frac{\mu_B g_F}{\hbar}$. For the cesium ground state, $F = 3$, the gyromagnetic ratio is $\gamma/2\pi = -3.5\,\mathrm{Hz/nT}$.

The Hamiltonian can further be written as $H_B = -\frac{\mu_B g_F}{\hbar} F_z B_z$ and the correction to the hyperfine energy is $E = -\mu_B g_F m_F B_z$. The energy difference between neighbouring Zeeeman sublevels, $\Delta m_F = 1$, is

$$\Delta E = \mu_B g_F B_z = \gamma \hbar B_z. \tag{3}$$

2.3 Larmor precession and Rabi oscillations

Magnetization of an atomic ensemble is defined as $\mathbf{M} = \frac{1}{V} \sum_i \boldsymbol{\mu}_i$, where the sum runs over all the atoms and V is the volume containing the atoms. In large ensembles the magnetization can be described classically [10].

The torque on a magnetic moment $\boldsymbol{\mu}$ in a magnetic field $\mathbf{B}$ is $\boldsymbol{\mu} \times \mathbf{B}$. According to Newton's second law this torque is equal to the time derivative of the angular momentum $\boldsymbol{\Gamma}$,

$$\frac{\mathrm{d}\boldsymbol{\Gamma}}{\mathrm{d}t} = \boldsymbol{\mu} \times \mathbf{B}. \tag{4}$$

By multiplying this equation with γ/V and taking into account the connection between the magnetic and angular moment $\gamma\boldsymbol{\Gamma} = \boldsymbol{\mu}$, we get Bloch's equation

$$\frac{\mathrm{d}\mathbf{M}}{\mathrm{d}t} = \mathbf{M} \times \gamma\mathbf{B}. \tag{5}$$

This equation describes Larmor precession of the magnetization around the direction of the external magnetic field with the Larmor angular frequency $\omega_0 = \gamma B$ where $B = |\mathbf{B}|$ is the magnitude of the applied magnetic field. The Larmor frequency corresponds to the energy difference between neighbouring Zeeman subleves $\Delta E = \hbar\omega_0$.

For the description of relaxation mechanisms, the Bloch equations have additional phenomenological terms that describe the deterioration of the signal with characteristic times T_1 and T_2. T_1 is the longitudinal relaxation time, the time in which magnetization relaxes into its equilibrium state in the direction of the magnetic field. T_2 is the transversal relaxation time, describing the decay of the transversal component of the magnetization.

The solutions of Bloch equations with the phenomenological relaxation terms, in case the magnetic field is constant in z-direction and the equilibrium magnetization is M_0, are

$$M_{xy} = M_x(0)e^{-i\omega_0 t}e^{-t/T_2},$$
$$M_z(t) = M_0 - (M_0 - M_z(0))e^{-t/T_1},$$

where $M_{xy} = M_x + iM_y$ [2].

Suppose we add an oscillating magnetic field in the x-direction. It can be treated as a sum of two circulating components

$$\mathbf{B}'(t) = 2B'(\cos\omega t, 0, 0) = B'(\cos\omega t, \sin\omega t, 0) + B'(\cos\omega t, -\sin\omega t, 0).$$

In a system with a static magnetic field B_z in z-direction it is simpler to describe magnetization in a rotating coordinate system where the x'- and y'-axes rotate around the z-axis with the angular frequency $\omega_0 = \gamma B_z$ and the z'-axis is the same as z. In this coordinate system the magnetization is static and is effectively not influenced by B_z. If the frequency of the additional oscillating magnetic field equals the Larmor frequency, one of its components is static in the rotating reference frame. The other one is oscillating with double the Larmor frequency and its contribution averages to zero. Because of the static component of the added magnetic field, the magnetization precesses around the x'-axis of the rotating coordinate system with the frequency $\Omega = \gamma B'$. This phenomenon is called Rabi oscillation and Ω is the Rabi frequency.

Starting from the equilibrium magnetization in the z-direction, the pulse of an oscillating magnetic field causes the magnetization to tilt from the z-axis for a certain angle, determined by the length of the pulse. Usually $\pi/2$ and π pulses are used. With a $\pi/2$ pulse the magnetization rotates from z-direction to the xy-plane. After a π pulse, the direction of the magnetization is the exact opposite of the initial magnetization. These pulses of the magnetic field are often referred to as RF pulses because in the experiments the Larmor frequency is in the radio-frequency range.

2.4 Stern-Gerlach method

Populations of m_F components after rotating a spin F from the initial state $m_F = F$ by an angle can be calculated by applying the rotation matrix to the initial vector. The probability that we measure an atom in a certain m_F state, depending on the angle of rotation, is shown in Figure 2, for $F = 3$. We can see that the only pure states we can get with a rotation are $m_F = F$ and $m_F = -F$. In any other case the state is a combination of multiple neighbouring m_F states.
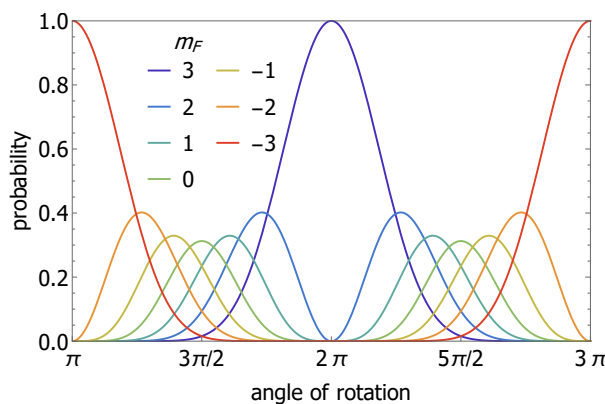

Figure 2. The population of each of the m_F components depending on the angle of rotation. Adapted from [2].

By placing an atom cloud in a magnetic field gradient, atoms in different Zeeman sublevels can be spatially separated. Usually a strong magnetic field gradient and a constant homogeneous

magnetic field in the vertical direction are applied. The constant homogeneous field ensures that the magnetic field has the same direction over the whole the cloud despite the gradient and the gradient separates the atomic cloud based on the quantum number m_F. That is because an inhomogeneous magnetic field acts upon a magnetic dipole moment with a force $\mathbf{F} = \boldsymbol{\mu} \cdot \nabla \mathbf{B}$ that is proportional to the projection of the magnetic moment onto the magnetic field gradient. In the case when not all the atoms are in the same magnetic sublevel, we observe multiple spatially separated clouds. This phenomenon was first used in the Stern-Gerlach experiment, that is why this type of measurement is called a Stern-Gerlach measurement.

From the measurement of the number of atoms in each of the Zeeman sublevels N_{m_F}, we can obtain the projection of the magnetization in the direction of the magnetic field gradient

$$M_z \propto \frac{\sum_{m_F} m_F N_{m_F}}{\sum_{m_F} N_{m_F}}. \tag{6}$$

3. Experiments

In this part of the article we present experimental observations of Rabi oscillations and Larmor precession using the Stern-Gerlach method and two ways of measuring the magnetic field gradient utilizing these phenomena. The experiments are done with cold cesium atoms held in an optical dipole trap.

We prepare a cloud of cold cesium atoms by laser cooling with the usual procedure, described in detail in [11], and transfer them to the dipole trap. There we have approximately $200\,000$ atoms at $1\,\mu\text{K}$. As a consequence of the previous cooling stage, the atoms are in the $|F = 3, m_F = 3\rangle$ state.

3.1 Rabi oscillations

Rabi oscillations occur when applying a magnetic field oscillating with the Larmor frequency in the direction perpendicular to the static magnetic field. We experimentally observe these oscillations with the following procedure. Starting with atoms polarized in the z-direction, we turn on the RF magnetic field in the x-direction with the frequency ω_0, that corresponds to the static magnetic field in the z-direction. After a certain amount of time the RF field is turned off and then the atoms are separated by their m_F with the Stern-Gerlach method and an absorption image of the atom clouds is taken.
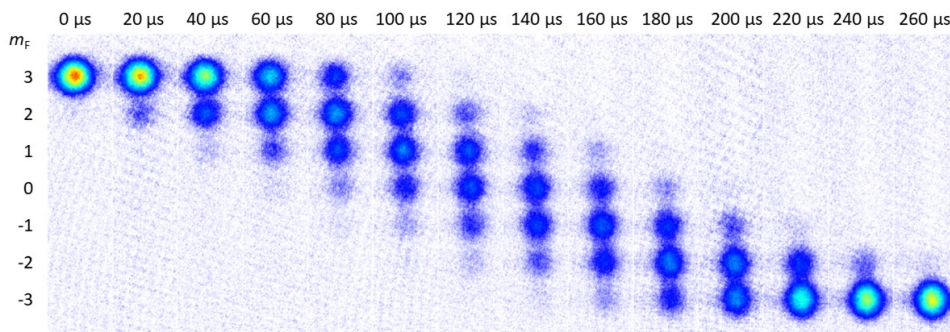

Figure 3. Absorption images of one half of a Rabi oscillation. The images show populations of each of the m_F states after a RF pulse. The length of the pulse is written above each image. Courtesy of Cold atom laboratory at Jožef Stefan Institute.

Images for increasing lengths of the RF pulses are shown in Figure 3. We determine the number of atoms in each of the 7 Zeeman sublevels of the cesium ground state and calculate the magnetization

projection using equation (6). The results in Figure 4a are used to determine the frequency of Rabi oscillations and the length of $\pi/2$-pulses in the following experiments.
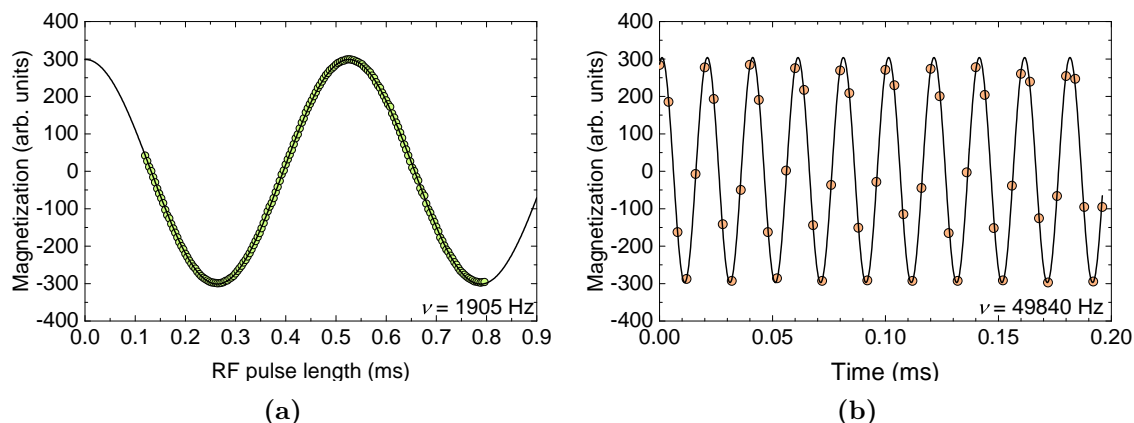

Figure 4. (a) The z-component of magnetization during Rabi oscillations. (b) Oscillations of the magnetization projection as a function of the interrogation time due to Larmor precession. On both graphs the dots are measurements and the black line is a sine function fitted to the data. Courtesy of Cold atom laboratory at Jožef Stefan Institute.
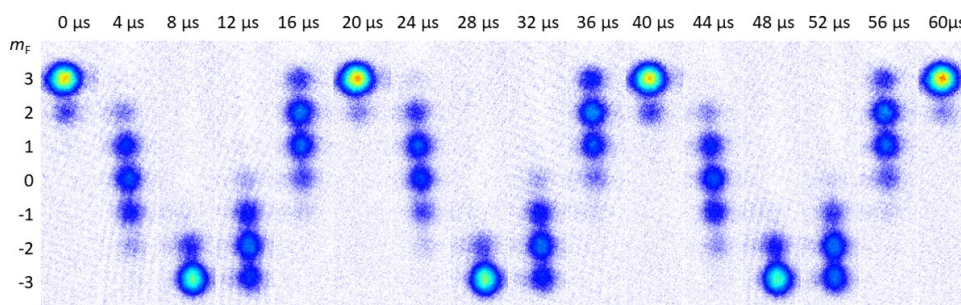
3.2 Larmor precession

Figure 5. Absorption images of Larmor precession. The time written above each image is the interrogation time. Courtesy of Cold atom laboratory at Jožef Stefan Institute.

To measure the Larmor precession we use the Ramsey sequence of RF pulses followed by a Stern-Gerlach measurement. A Ramsey sequence consists of two $\pi/2$ pulses separated by the interrogation time t. With the first pulse the magnetization is rotated from the z-direction to the xy-plane, where it is then left to precess until the second $\pi/2$ pulse. The second pulse rotates the spin around the x-axis, so the y-component becomes the z-component of the spin. Then we perform a Stern-Gerlach measurement to measure the z-projection of the magnetization, that corresponds to the the y-projection at the start of the second $\pi/2$ pulse. By varying the time between the two pulses, we observe the oscillations of the projection with the frequency of Larmor precession. The absorption images are shown in Figure 5 and the magnetization as a function of time in Figure 4b.

3.3 Gradiometry with two atom clouds

To measure a component of the magnetic field gradient we simultaneously perform the measurement of Larmor precession on two atom clouds. From the phase difference between them the difference in the magnetic field is determined.
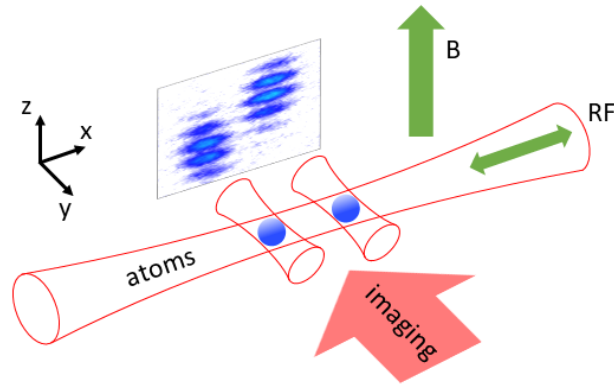
Figure 6. Schematic illustration of the experimental setup for the experiment with two atom clouds, that are in dipole traps. The directions of the imaging beam and the static and RF magnetic fields are shown.

Each of the clouds consists of approximately $200\,000$ atoms and the clouds are separated by approximately $300\,\mu\text{m}$. The experimental setup is schematically shown in Figure 6. Because the magnetic field is not homogeneous, the precession frequencies are not the same for the first and the second cloud. All atoms start with the same phase, but with time, the phase difference accumulates as

$$\begin{aligned} \phi(t) &= \omega_2 t - \omega_1 t \\ &= \gamma \left(B(\vec{r_2}) - B(\vec{r_1}) \right) t \\ &\approx \gamma t \left(\vec{r_2} - \vec{r_1} \right) \cdot \nabla B. \end{aligned} \tag{7}$$

The phase difference is therefore a measure of the derivative of the magnetic-field strength B along the axis of the two probes x. In our case $B = B_z$, $d = |\vec{r_2} - \vec{r_1}|$ and we can write

$$\frac{\partial B_z}{\partial x} = \frac{\phi}{\gamma t d}. \tag{8}$$
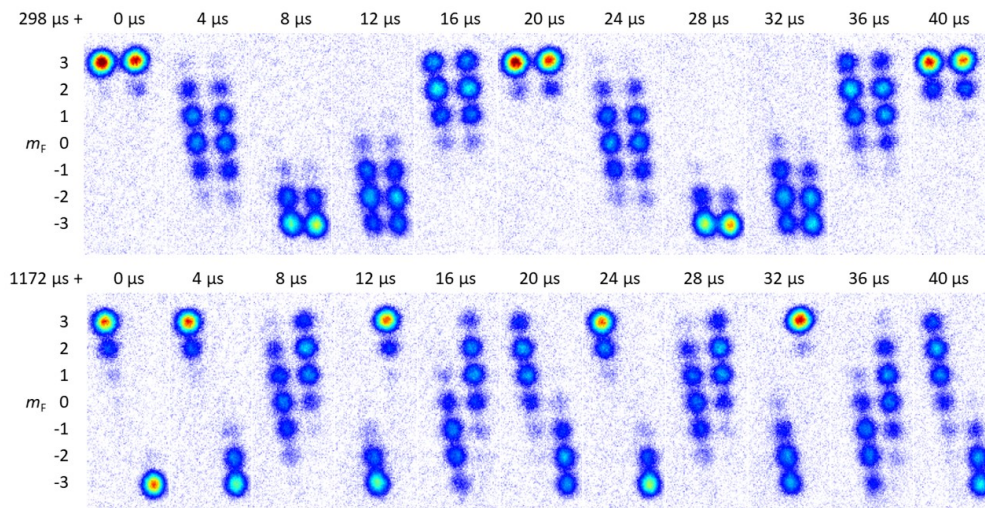

Figure 7. Absorption images of Larmor precession of two atom clouds. The first image shows the two clouds precessing in-phase. The bottom image shows the clouds at longer interrogation times, when the clouds are out of phase. Courtesy of Cold atom laboratory at Jožef Stefan Institute.

In Figure 7 we show an example of two atoms clouds precessing in and out of phase, i. e., with the phase difference π. There are two ways of determining the phase difference from the

measurements. We use the simpler option where the phase difference is determined by fitting a sine function to the measured magnetization. In the fit the frequency is kept constant and the phase is determined as a function of time for each atom cloud separately. The other option is to fit an ellipse to parametric plot of the magnetization of the two clouds as in Ref. 6. On the horizontal axis we put the magnetization of the first cloud and on vertical axis the magnetization of the second cloud. For measurements that differ very little in the interrogation time, the phase difference is practically constant and the points on this parametric plot trace an ellipse, from which a phase difference is obtained. Examples of these ellipses for different phase differences are shown in Figure 8. In both approaches, the accumulated phase difference can not be determined without the whole time dependence from the start, otherwise it could differ from the measured phase for a multiple of 2π.
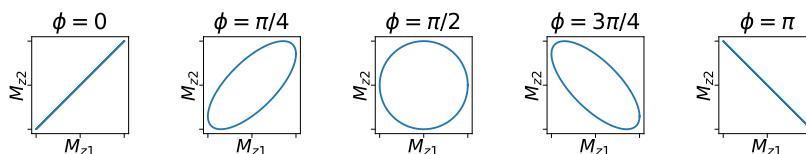

Figure 8. The relative phase between the two probes can be calculated from the shape of the ellipse that is the parametric plot of the magnetizations: $M_{z1} \propto \sin(t)$, $M_{z2} \propto \sin(t + \phi)$.
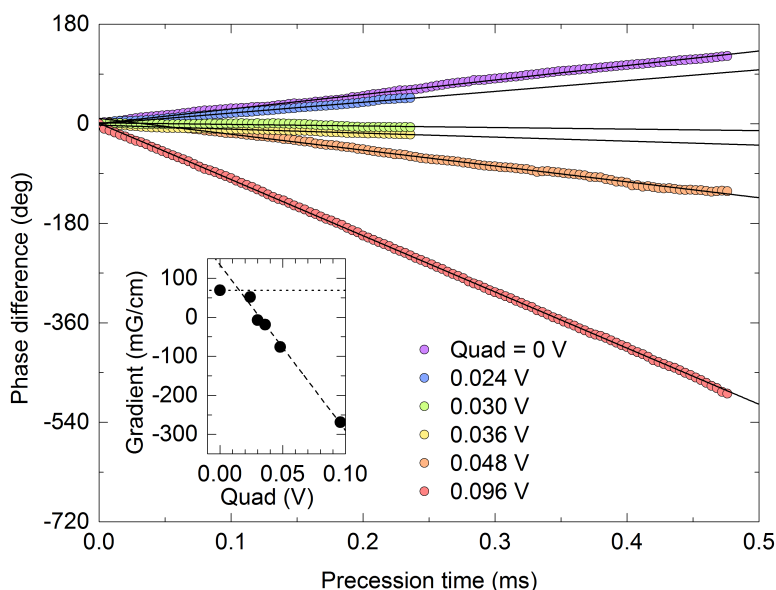

Figure 9. Phase difference between the two atom clouds is a linear function of time and the magnetic field gradient is proportional to the slope. The measurements were done in different gradients created by different voltages on the quadrupole coil. Courtesy of Cold atom laboratory at Jožef Stefan Institute.

We plot the time dependent phase in Figure 9 and fit a linear function to the experimental data. The gradient is calculated from the slope of the linear function using equation (8). The different colored measurements are for different voltages on the quadruple coil in the x-direction, which creates the gradient. In the insert the measured magnetic gradient is plotted as a function of the quadrupole coil voltage.

3.4 Gradiometry with an elongated atom cloud

The method of measuring the magnetic field gradient with two atom clouds has many flaws. A series of measurements is needed, because the whole evolution of the phase difference is required. Additionally, the analysis of the measurements is complicated, especially if using the ellipses to determine the phase difference. A better way to measure the magnetic field gradient is the measurement of position dependent Larmor precession on an elongated atom cloud. This way the phase is measured as a function of the position and the gradient can be determined from a single shot.

A magnetic field gradient causes the precession phase to change along the cloud. Using the linear approximation for the position dependence of the magnetic field $B(x) \approx B_0 + \frac{\partial B_z}{\partial x}x$ we can write the magnetization as a function of the time and the position as

$$M_z(x,t) = M_0 \cos\left(\gamma B_0 t + \gamma \frac{\partial B_z}{\partial x}xt\right). \tag{9}$$
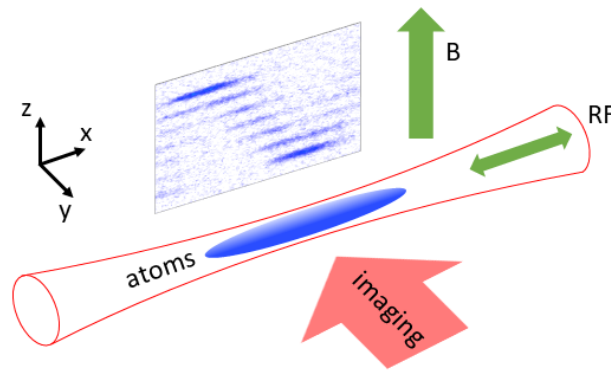

Figure 10. Schematic illustration of the experimental setup for the experiment with an elongated atom cloud, showing the direction of the static and RF magnetic fields and the direction of the imaging beam.

In the experiment the atoms are cooled the usual way in an optical trap that is made by two crossed laser beams. To create an elongated atom cloud one of them is turned off and the cloud expands along the remaining beam, as it is shematically shown in Figure 10. Then the same experimental sequence is used as in the previously described experiments. We take an absorption image and from it the magnetization as a function of the position is calculated. Both are shown in Figure 11. We fit the theoretical function $\cos(kx + \phi)$ to the measured magnetization, to determine the wave number $k = \gamma \frac{\partial B_z}{\partial x}t$. Since the interrogation time t is known we get the gradient $\frac{\partial B_z}{\partial x}$ from a single image.

We test the accuracy of our measurement by repeating the same experiment multiple times and for different interrogation times. The results are shown in Figure 12 where we plot the wave number k as a function of the interrogation time. We get a better estimate of the true value of the gradient by fitting a linear function and calculating the gradient from the slope. The measurements should lie on a line that goes through the origin, but for our measurements this is not the case. This means that the initial magnetization has some spatial dependence. That could be a result of the inhomogeneity of the RF magnetic field. Additionally, we see that the measurement for the longer interrogation time lies below the line of the other dots. This could be because, in our analysis, we do not take into account the fact that the cloud is still expanding during the experiment.

Even for non-expanding atom clouds the range of interrogation times suitable for this experiment is limited. In principle the precision of the measurement of k is higher for longer interrogation times, where we get more periods of the magnetization projection oscillation along the cloud. But for longer interrogation times the spatial resolution decreases, because it is limited by the diffusion of the atoms during that time.
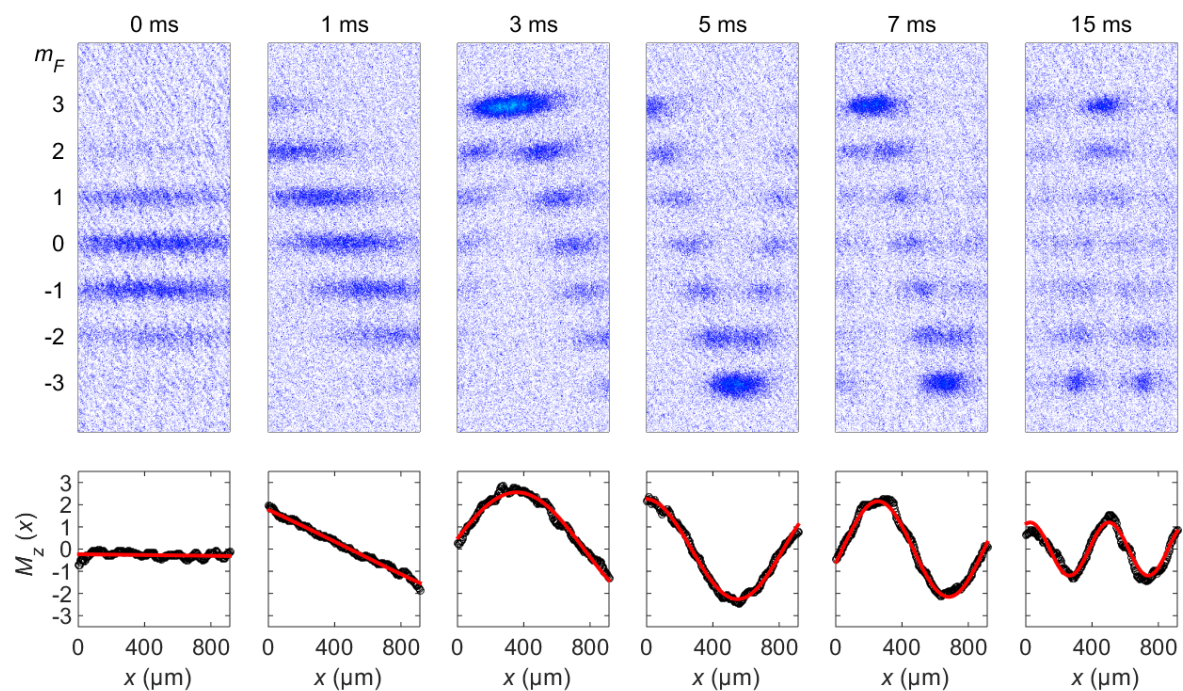
Figure 11. Absorption images of the Stern-Gerlach measurement of an elongated atomic cloud after different interrogation times. Below, the magnetization projection is plotted as a function of position. In red the sine function fit to the measurements is shown. Courtesy of Cold atom laboratory at Jožef Stefan Institute.
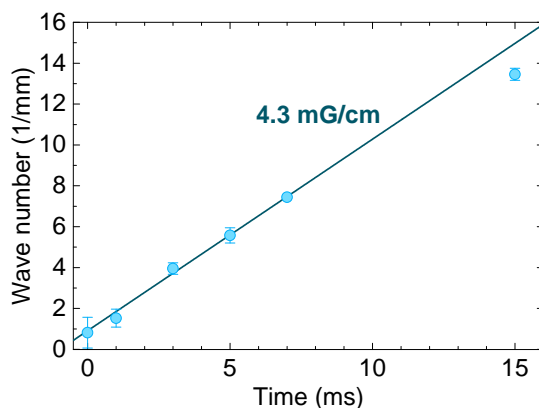

Figure 12. The measured wave number as a function of the interrogation time. Courtesy of Cold atom laboratory at Jožef Stefan Institute.

4. Conclusion

In conclusion, we demonstrate a single-shot method of measuring a component of the magnetic field gradient. The magnetic field is probed through the Larmor precession of atomic magnetization, that is detected via the Stern-Gerlach method. The use of an elongated atom cloud utilizes the high spatial resolution of cold atoms to probe the spatial dependence of the magnetic field. In contrast to the method with two atom clouds, the temporal dependence of the magnetization is not needed to determine the magnetic field gradient, making the measurement simpler and quicker.

References

[1] D. Budker and M. Romalis. Optical magnetometry. *Nature Physics*, 3(4):227–234, 2007.

[2] T. Arh. Nedestruktivno slikanje in magnetometrija s Faradayevo rotacijo v plinu cezijevih atomov. Master's thesis, University of Ljubljana, 2019.

[3] Y. Eto et al. Spin-echo-based magnetometry with spinor Bose-Einstein condensates. *Physical Review A*, 88(3):031602, 2013.

[4] M. Koschorreck et al. High resolution magnetic vector-field imaging with cold atomic ensembles. *Applied Physics Letters*, 98(7):074101, 2011.

[5] J. Lenz and S. Edelstein. Magnetic sensors and their applications. *IEEE Sensors journal*, 6(3):631–649, 2006.

[6] A. A. Wood et al. Magnetic tensor gradiometry using Ramsey interferometry of spinor condensates. *Physical Review A*, 92(5):053604, 2015.

[7] Y. Eto et al. Control and detection of the Larmor precession of F=2 ^{87}Rb Bose–Einstein condensates by Ramsey interferometry and spin-echo. *Applied Physics Express*, 6(5):052801, 2013.

[8] J. M. Higbie et al. Direct nondestructive imaging of magnetization in a spin-1 Bose–Einstein gas. *Physical Review Letters*, 95(5):050401, 2005.

[9] D. A. Steck. Cesium D line data. Available online at `http://steck.us/alkalidata` (revision 2.2.1, 21 November 2019).

[10] C. P. Slichter. *Principles of magnetic resonance*, volume 1. Springer-Verlag Berlin Heidelberg, 1990.

[11] T. Mežnaršič. Lasersko hlajenje cezijevih atomov. Master's thesis, University of Ljubljana, 2016.